Simultaneous removal of Cr(VI) and orange G6 by polyaniline/attapulgite supported nano zero-valent iron activate persulfate

Hui Xu*, Lei Tian, Yajuan Zhang, Ming Zhang Chen, Xudong Jiang, Weiguo Tian, Yong Chen*

College of Petrochemical Technology, Lanzhou University of Technology, Lanzhou, China, Tel. +86-931-2975872;
emails: xuhui@lut.cn (H. Xu), chenylut@126.com (Y. Chen), 2528989045@qq.com (L. Tian), 1799797925@qq.com (Y.J. Zhang),
1377380676@qq.com (M.Z. Chen), 1020990948@qq.com (X.D. Jiang), 3047007413@qq.com (W.G. Tian)

ABSTRACT

In this paper, the polyaniline/attapulgite composite supported nano zero-valent iron (nZVI/PANI/APT) composites were synthesized by one-step oxidation using Fe^{3+} as oxidant and iron source. nZVI/PANI/APT was used as a catalyst to activate persulfate (Ps) for the simultaneous removal of Cr(VI) and orange G6 (OG6) from aqueous solutions. The main factors (different composite materials, pH value, Ps concentration, etc.) affecting the removal performance of Cr(VI) and OG6 were evaluated as well. The experimental results revealed that the nZVI/PANI/APT composites can effectively remove Cr(VI) and OG6 simultaneously at a relatively low Ps concentration, the removal efficiencies of Cr(VI) and OG6 were 99.7% and 99.4% after 60 min, respectively. PANI/APT as the supporter matrix could decrease the aggregation of nZVI and increase its reactivity. A good synergistic effect between Cr(VI) reduction and OG6 oxidation was achieved by nZVI/PANI/APT combined Ps system. nZVI not only can be as a reductant for removal Cr(VI) and OG6 but also play as a catalyst to activate Ps and generate radicals for the degradation OG6. The presence of persulfate could not significantly decline nZVI reactivity for Cr(VI) reduction but remarkably promote OG6 oxidation. Moreover, kinetic and thermodynamic analyses were used to study the removal process, and the possible removal mechanism of Cr(VI) and OG6 was discussed by using the UV-Vis spectrum and liquid chromatography-mass spectrometry techniques. The nZVI/PANI/APT-persulfate heterogeneous Fenton system combines the nZVI reduction with the Fenton-like oxidation, which can be used for the treatment of industrial wastewater containing heavy metal ions and organic dyes.

Keywords: Nano zero-valent iron; Persulfate; Simultaneous removal; Orange G6; Cr(VI)

1. Introduction

In recent decades, with the rapid development of industry, the co-existence of multiple contaminants is a common phenomenon in the actual wastewater, which greatly increases the risk to the environment and human health [1–3]. Among various pollutions, Cr(VI) and azo dyes (–N=N– unit as the chromophore) as two kinds of representative pollutants which often originate from industrial sources of wastewater, such as leather tanning, photographic-film making, car manufacturing, petroleum refining due to their highly toxic, non-biodegradation and more potential carcinogenic risk must be cautiously used.

The main problem of these wastewater treatments is that these contaminates have significant differences in molecular structure, molecular weight, composition and toxicity [4], which has led to the inability of conventional adsorbents to simultaneously remove of organic compounds and

* Corresponding authors.

heavy metals meet emission standards. Biology, adsorption, chemical oxidation, visible light photocatalysis, advanced oxidation processes (AOPs) and other technologies have been widely used in the removal of complex pollutants in wastewater [5–8]. Recently, AOPs are considered to be an effective way for the degradation of organic dyes. Most AOPs generally used hydroxyl radical HO$^•$ (E_0 = 2.8 V) as the main oxidant to remove toxic and refractory organic pollutants, while Fenton's reagent persulfate (Ps), a strong two-electron oxidizing agent with a redox potential of 2.01 V, has examined to be efficient for removal dyes [9]. Moreover, activation of Ps by transition metal ions to generate reactive (SO$_4^{•-}$) with a redox potential of 2.6 V [10–12] which can oxidize most of the organic pollutants in water [13]. Commonly, Ps can be activated by transition metal ions such as Co$_x$O$_y$, MnO$_2$, etc. to generate a stronger non-selective oxidant sulfate radical anions (SO$_4^{•-}$) [14,15]. Among these activators, the Fe^{2+} aqueous solution is the most preferable application for environmental treatment since other metal ions are toxic. Azo dyes and Cr(VI) reduction by nano zero-valent iron (nZVI) has been reported to be one of the most promising treatment due to its high surface area and strong reductive capability. Although the chromophoric structure –N=N– of azo dye was currently cleavaged by nZVI commonly, it is difficult to make intermediate products of azo dyes degrade more non-toxic small molecules. The removal process may take more time or combine with the Fenton reaction [14]. There are some researches about the activation of persulfate by nZVI to generate sulfate radical anions to remove organic compounds in heterogeneous nZVI-Ps Fenton-like system [9,16] demonstrate that nZVI could slow the release of Fe^{2+}, which can activate persulfate, producing sulfate radical anions oxidation to the removal of organic compounds. The use of nZVI can overcome the shortcomings of Fe^{2+}, and avoid the introduction of other anions. This heterogeneous nZVI-Ps system combines nZVI reduction with Fenton-like oxidation aroused more interest in the degrade organic pollutants and removes heavy metal ions [17].

Nevertheless, nZVI usually tents to aggregate inevitably leading to the decrease of the reduced ability of nZVI and catalytic activity of Ps, and powder catalysts are difficult to separate from the treated water. To solve these defects, some supporting materials were introduced to improve the dispersion and stability of nZVI, and nZVI particles are supported or modified on substrates to change nZVI particle surface characteristics. Various types of supported or modified nZVI have been used for the removal of dyes and heavy metals, such as kaolinite-supported nZVI, bentonite-supported nZVI, sepiolite-supported nZVI and polymeric resin-supported, etc. [18–21]. Among these supporters, the clay mineral attapulgite (APT) can be used for the immobilization of nZVI due to its abundant, large surface area and adsorption capability [2]. APT is widely used as a low-cost adsorbent for the removal of metal ions and organic pollutants [22,23]. Despite the comparatively the low-cost of APT, APT still suffers from poor adsorption capacity and difficult to reuse. A feasible solution is to use a stable substrate with abundant active sites to combine clay nanomaterial to increase its adsorption efficiency [24,25].

Conductive polymer polyaniline (PANI) with linear macromolecule chains, has abounded amine and imine functional groups, which exhibit good adsorption of various pollutants and electrical conductivity [24]. In our previous study, PANI composites APT as supporters could effectively decrease the aggregation of zero-valent iron particles, and enhanced its reactivity and improving adsorption capacity for remove Cr(VI) and azo dye [26]. Moreover, as far as we know, there are few studies about the effectiveness of the nZVI/PANI/APT-Ps Fenton-like process in the removal of Cr(VI) and orange G6 (OG6) simultaneously in literature. Therefore, it appears significant to investigate the removal efficacy for specific pollutants of the novel composites.

In this study, PANI/APT composite carrier was used to support and modify nZVI, and simultaneous removal performances of Cr(VI) and OG6 by nZVI/PANI/APT composite in the presence of Ps were investigated at various conditions. The effect of Ps in the system was elucidated and the proposed degradation pathways of Cr(VI) and OG6 were also analyzed. In addition, the experimental parameters of adsorption thermodynamics and kinetics models provided the basis for the removal mechanism analysis. The research combines the reduction of nZVI with the Fenton oxidation reaction, removal of Cr(VI) and azo dyes by nZVI reduction, and slowly releases Fe^{2+}. The Fe^{2+} activated persulfate decomposes to produce strong oxidizing sulfate radical anions, and oxidative degradation of the organic dye OG6. We try to develop a novel composite to remove efficiently heavy metals and organic dyes simultaneously.
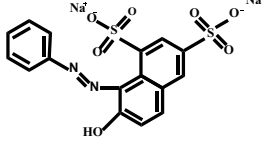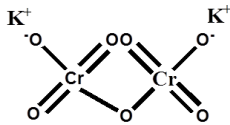
2. Experimental setup

2.1. Materials

Attapulgite (99%, APT) (JC-J503) was purchased from Jiangsu Xuyi Nano-Materials Science and Technology Co., Ltd., China. All chemical reagents (NaBH$_4$, H$_2$SO$_4$, HCl, NaOH and FeCl$_3$·6H$_2$O) used in this study were of AR grade. FeCl$_3$·6H$_2$O was purchased at Tianjin Shuangchuan Chemical Reagent Factory, China. Aniline was supplied by Sinopharm Chemical Reagent. OG6 was offered by the Shanghai Yuanye Biotechnology Co., Ltd., China.

2.2. Preparation of nZVI/PANI/APT and nZVI/APT

The nZVI/PANI/APT composite was synthesized by a one-step oxidation method using APT as a dispersant. In a 250 mL beaker, 1 g of APT was ultrasonically stirred in 80 mL of distilled water for 20 min at first, and then 7.24 g of FeCl$_3$·6H$_2$O was added to dissolve it and 0.8 ml of aniline was quickly added under magnetic stirring, which was stirred for 5 min and then let stand for 24 h. The above mixture was added to a 250 mL three-necked flask, and a freshly prepared sodium borohydride solution (1.89 g dissolved in 100 mL of distilled water) was added dropwise under a nitrogen atmosphere. After completion of the dropwise added, stirring was continued for 20 min, suction filtration, washing three times with absolute ethanol, and vacuum drying at 65°C for 12 h to obtain an nZVI/PANI/APT composite material. The preparation process of the nZVI/APT composite material was the same as described above except that no aniline was added, and nZVI was prepared under identical conditions but without APT and aniline.

Table 1
General characteristics of Cr(VI) and OG6

	Molecular weight	λ_{max} (nm)	Structure
Orange G6 (OG6)	452.37	475	
Cr(VI)	294.21	540	

2.3. Experimental procedures and analytical methods

Sixty milliliters of a mixture of Cr(VI) and OG6 with an initial concentration of 30 mg L^{-1} was placed in an Erlenmeyer flask to adjust the pH of the solution to 3 (adjusted by 0.1 M hydrochloric acid and 0.5 M sodium hydroxide solution). The adsorbent nZVI/PANI/APT was added to an amount of 60 mg and the persulfate concentration was 2 mM. The mixture was shaken in a gas bath thermostat for 120 min at temperature 298 K. The reaction solution was filtered through a filter at regular intervals. As shown in Table 1, the concentration of Cr(VI) was determined by the 1,5-diphenyl-carbazide colorimetric method monitoring the absorbance at 540 nm in acidic solution with a UV-Vis spectrophotometer. The concentration of dye OG6 was measured using a UV-Spectrophotometer at $\lambda = 475$ nm. Although the characteristic peaks of Cr(VI) (540 nm) and OG6 (475 nm) are adjacent, the concentration of Cr(VI) and OG6 measured with an UV-Spectrophotometer is accurate. As shown in the curve of Fig. S1 in the supplementary information, it is the UV-Vis spectrum of OG6 and Cr(VI) alone and before the reaction of the mixture. In this study, the persulfate solution 1–4 mM was prepared, compared to the removal efficiencies of OG6 and Cr(VI) when the presence or absence of persulfate.

The removal efficiency of the contaminant and adsorption capacity was calculated by the following equations:

$$R(\%) = \frac{C_0 - C_t}{C_0} \times 100 \tag{1}$$

$$q_t = \frac{C_0 - C_t}{m} \times V \tag{2}$$

where $R(\%)$ is the removal efficiency of the pollutants; q_t is the adsorption capacity of the dye at t min; C_0, C_t are the initial concentration of the pollutant solution and the concentration at t min (mg L^{-1}); V is the volume of the adsorbate solution (L); m is the mass of the adsorbent (g).

In order to provide some instructions through testing, we conducted the following tests on the simple of nZVI/PANI/APT: Scanning electron microscopy (SEM) images, X-ray photoelectron spectroscopy (XPS) spectra, transmission electron microscopy (TEM) images, X-ray diffraction (XRD) patterns were respectively obtained on a JSM-6701F (JEOL, Japan), a K-alpha ESCALAB 250Xi instrument (Therm Fisher-VG Scientific, USA), with Al Kα radiation as the excitation source, which the binding energies were corrected for specimen charging by referencing C 1s (284.8 eV), a JEM-1200EX (FBI, America) and D/MAX-2400X (Rigaku, Japan). A nitrogen adsorption–desorption isotherm at 77 K was measured on an ASAP 2020 absorption analyzer (Micromeritics, America), from which the specific surface area and the pore size distribution of the samples were deduced using the Brunauer–Emmett–Teller (BET) method and the Barrett–Joyner–Halenda method. LC-MS identified OG6 degradation products. The capillary column is a reversed-phase column C-18 (100 mm × 2.8 mm). The particle size of the packing is 3 μm. The mobile phase is a mixture of acetonitrile-water and its gradient elution range from 20/80 (v/v) to 80/20 (v/v) by stepwise change. The flow rate of the eluent was 0.08 mL min^{-1}, and the sample injection volume was 20 μL. The MS analysis was set in the negative ion scanning mode with a range of 50–500 m/z. The above is the general procedure of liquid chromatography-mass spectrometry (LC-MS).

3. Results and discussion

3.1. Characterization of synthesized samples

The XRD patterns of the nZVI, nZVI/APT, and nZVI/PANI/APT composites were shown in Fig. 1a. The nZVI showed a weak and a broad peak at about $2\theta = 44.6°$, which corresponded to the (110) crystal plane of body-centered cubic Fe^0 [27], indicating nZVI was successfully prepared. The characteristic peaks of APT were at $2\theta = 8.6°$, 26.6°, and 35.2° [28]. The high-intensity diffraction peak at $2\theta = 31.2°$ which is attributed to quartz impurity of APT [29]. Meanwhile, the diffraction characteristic peaks of nZVI ($2\theta = 44.6°$), APT ($2\theta = 8.6°$) and PANI (20.76°) appear in the nZVI/PANI/APT composites [30], declaring that nZVI is already loaded on dispersant APT/PANI. Simultaneously, the new diffraction peak at $2\theta = 62.8°$ was corresponded to the (440) crystal planes of Fe_3O_4 [31], implying that the nZVI surface partly was oxidized to form iron oxide.

Fig. 1b shows the Fourier-transform infrared spectroscopy (FTIR) spectra of APT, PANI, nZVI/PANI/APT
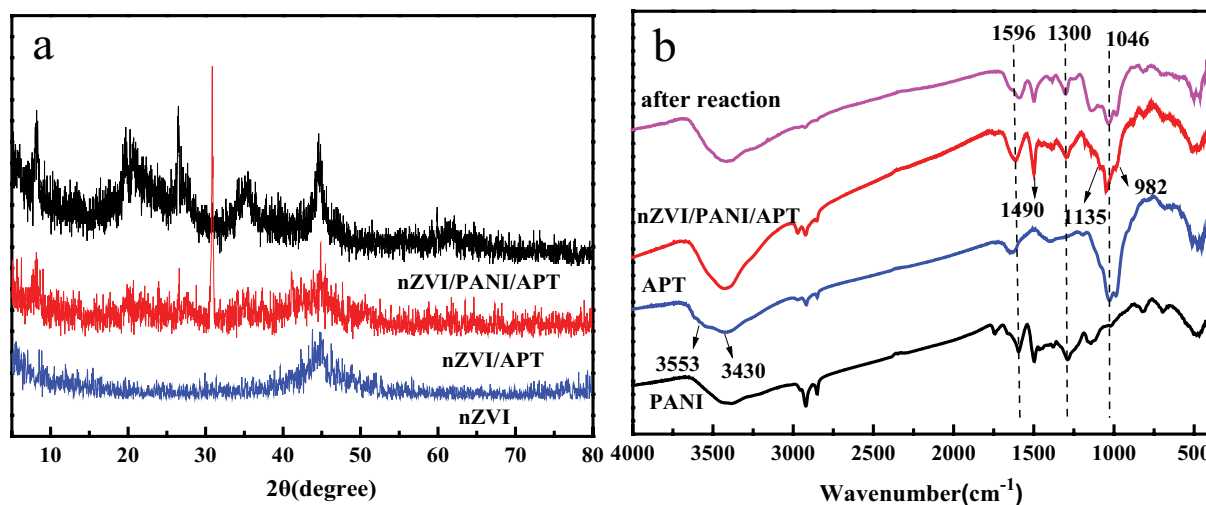
Fig. 1. (a) XRD patterns of nZVI, nZVI/APT and nZVI/PANI/APT and (b) FTIR spectra of APT, PANI, before and after reaction nZVI/PANI/APT with Cr(VI) and OG6.

composites before and after reaction with OG6 and Cr(VI). The strong absorption peaks at 3,553 and 3,430 cm^{-1} belong to the –OH group in the APT, which are the stretching vibration peak of structural water and superficially adsorbed water [32,33]. The bulk structure of the APT was shown by the stretching vibration peaks at 1,046 and 982 cm^{-1}, which correspond to the Si–O–Si bond and the (Mg, Al) –Si–O stretching vibration, respectively [34]. From the spectra of nZVI/PANI/APT and PANI composites, it can be seen that the absorption peaks at 1,596 and 1,490 cm^{-1} were attributed to the quinone structure C=C and the benzene structure C=C in PANI, respectively. The absorption peaks at 1,300 and 1,135 cm^{-1} corresponds to benzoquinone structure C–N stretching vibration and quinone-type structure N=Q=N stretching vibration. The absorption peaks at 1,583; 1,490 and 1,300 cm^{-1} were corresponded to the main structure of PANI [35,36]. After the reaction with OG6 and Cr(VI), the bands at 3,430; 1,596 and 1,049 cm^{-1} shifted to lower frequencies at 3,413; 1,581 and 1,033 cm^{-1}, respectively, whereas the peak at 1,135 cm^{-1} slightly shifted to a high-frequency band at 1,149 cm^{-1}. These changes indicated that these groups have an effect on the removal of the OG6 and Cr(VI).

The surface morphology images of the nZVI and nZVI/PANI/APT composites were evaluated by TEM. As shown in Fig. 2a, it has shown that spherical nZVI particles seriously aggregate and form prominent chain-like aggregates because of the magnetism reaction between the particles and the surface tension. The nZVI granules in Fig. 2b were obviously dispersed, nZVI coated on PANI sheets was well dispersed on the surface of APT and the size of the particles was in the range of several nanometers. The result demonstrated that APT/PANI as a support material was effective in reducing the aggregation and improving the dispersion of nZVI.

Figs. 2c and d exhibit SEM images of the APT/PANI and nZVI/PANI/APT composite, respectively. As can be seen from Fig. 2c, the rod-like structure of the APT was uniformly dispersed and the rough and porous surface was coated with PANI. Fig. 2d shows that the nZVI particles wrapped with PANI intertwined together and adhered to the surface of rod-like APT. The obtained result was consistent with the TEM images.

The XPS spectrums of nZVI/PANI/APT composites before and after reaction with pollutions were performed in Fig. 3. The peaks at 709.7 and 719.2 eV were belonging to the Fe^0, indicating the composites nZVI/PANI/APT were successfully synthesized. The photoelectron peaks at 711.0 and 712.6 eV are the 2p3/2 binding energy of iron oxide Fe(II)/Fe(III) and Fe(III), and 724.9 eV is the 2p1/2 binding energy of iron oxide Fe(III). The Fe(III) and Fe(II) was existence to confirm that parts of nZVI were oxidized before reaction and form a thin protective layer on the adsorbent surface. After the reaction, the peak at the 709.7 eV was disappearing and the peak at the 719.2 eV was significantly weakened to indicate nZVI participated in the removal of OG6 and Cr(VI). Meanwhile, the percentage of iron decreased from 23.62% before the reaction to 6.11%, which once again declare the nZVI was playing an important part in the reaction process. The peaks at 581.5 and 590.82 eV corresponded to the Cr(VI) 2p and the peaks at 577.5 and 587.2 eV belonged to the Cr(III) 2p, which indicated that Cr(VI) was converted to Cr(III) during the reaction process [37]. And also the total peak intensities of Cr(VI) were 5.8% and the Cr(III) was 94.2%. All the results indicated that Cr(VI) was adsorbed on the surface of APT/PANI and reduced to Cr(III) by nZVI.

In order to demonstrate the dispersion of nZVI after supported by APT/PANI, N$_2$ adsorption–desorption was studied and displayed in Table 2. S_{BET} of nZVI, nZVI/APT, and nZVI/PANI/APT were 17.51, 54.2, and 130.48 m^2 g^{-1}, respectively. Compared with nZVI, S_{BET} of nZVI/PANI/APT was almost 7 times more than nZVI, confirming that coating nZVI with APT/PANI immensely increased the surface area. Moreover, the pore volume of nZVI/PANI/APT was much higher than that of nZVI and nZVI/APT. These results suggested that the processing of loading APT/PANI increased the surface area and effectively improved the dispersion of nZVI. All these characteristics will
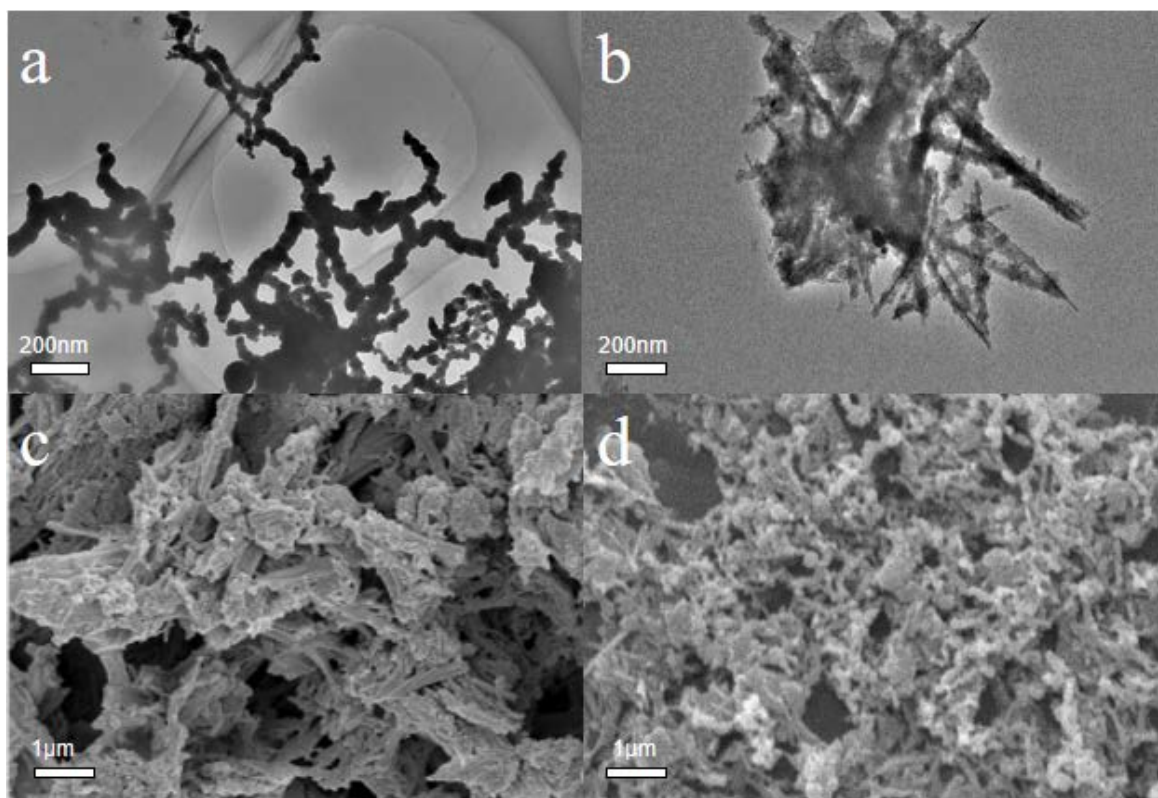
Fig. 2. (a) TEM images of nZVI, (b) nZVI/PANI/APT composites, (c) SEM images of APT/PANI, and (d) nZVI/PANI/APT composites.

Table 2
BET data of the synthesized samples

Samples	S_{BET} (m² g⁻¹)	V (m³ g⁻¹)	D (nm)
nZVI	17.51	0.045	10.39
nZVI/APT	54.20	0.132	9.76
nZVI/PANI/APT	130.48	0.267	8.19

promote pollutant removal efficiency, which mainly due to the porous structure of APT and improvement dispersion of nZVI.

3.2. Parameters affecting removal of Cr(VI) and OG6

3.2.1. Removal of Cr(VI) and OG6 by different synthesized samples

At 298 K, the concentration of persulfate was 2 mM, the effects of synthesized samples nZVI, nZVI/APT, and nZVI/PANI/APT on removal Cr(VI) and OG6 were shown in Fig. 4. As presented in Fig. 4a, the removal efficiencies of Cr(VI) by nZVI/APT and nZVI/PANI/APT were more than 95.0% after 90 min, while only 41.1% by nZVI. The results indicated that the reactivity of nZVI can be obviously improved since PANI/APT or APT could as supporter material to prevent nZVI from aggregation. The removal of Cr(VI) is mainly due to the redox reaction of nZVI and Cr(VI) in an acidic environment to cause decomposes into less toxic Cr(III) via Eqs. (1) and (2) [18]. As shown in Fig.

4b, the removal efficiencies of OG6 by nZVI, nZVI/APT and nZVI/PANI/APT were 95.3%, 98.3%, and 99.4% after 90 min, respectively. It was observed that the removal efficiency of OG6 by nZVI/PANI/APT was highest; suggesting that nZVI/PANI/APT in the presence of Ps exhibited a high reactivity toward OG6 oxidation. The high removal efficiency may be attributed to that nZVI reacts with Cr(VI) to produce Fe^{2+} under acidic conditions, and then Fe^{2+} can activate persulfate to produce sulfate radical anions, which further oxidize and degrade OG6 to mineralize into some inorganic compounds [11]. In addition, OG6 may be reduced by nZVI/PANI/APT, where nZVI was first oxidized and provided electrons, and then the dye molecule accepted electrons to break the –N=N– bond, thereby destroying the chromophore of the dye molecule for decolorization [16,34].

3.2.2. Effect of pH on the removal of Cr(VI) and OG6

The pH value of the solution is the main factor affecting the removal of Cr(VI) and OG6 and controlling the catalytic activity of Ps. The impact of pH on the removal of Cr(VI) and OG6 using nZVI/PANI/APT in the presence of Ps is shown in Fig. 5. When the reaction time was 60 min, the removal rate of Cr(VI) was close to 100% at pH = 3. The removal rate of Cr(VI) decreased at the pH range of 3–7, but a dramatic increase occurred at a pH range of 7–10. Approximately over 94.0% of Cr(VI) was removed after 60 min at a pH range of 3–4, whereas only 79.8% of Cr(VI) removal was obtained at pH = 10, which indicates that a strong acidic medium is a benefit to removal Cr(VI).
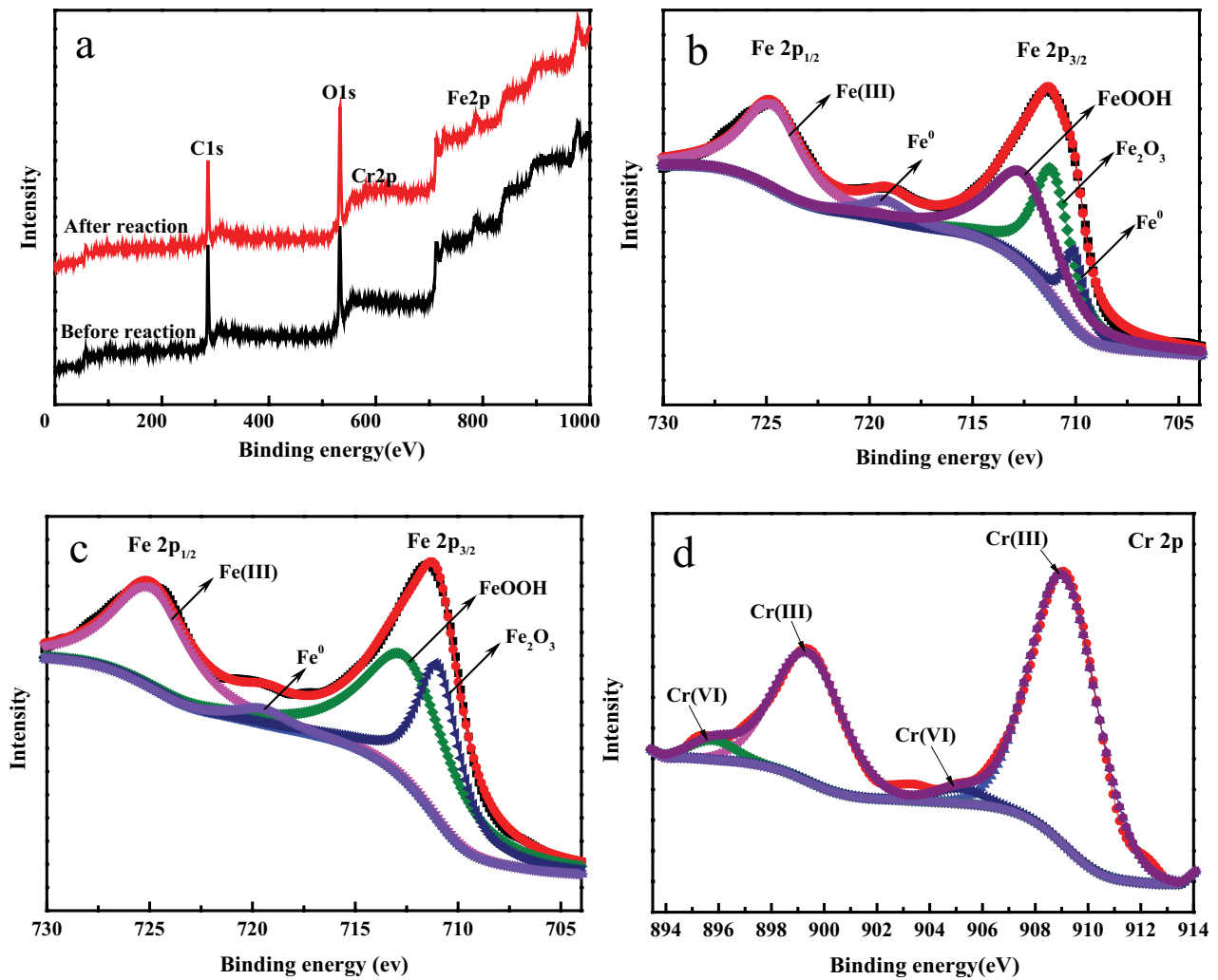
Fig. 3. XPS spectra of nZVI/PANI/APT (a) full spectra, (b) Fe2p before reaction, (c) Fe2p after reaction, and (d) Cr2p after reaction.

Table 3
Adsorption kinetics parameters of Cr(VI) and OG6

| Adsorption (mg L^{-1})	OG6 C_0 (mg L^{-1})			Cr(VI) C_0 (mg L^{-1})		
	50	100	150	50	100	150
Pseudo-first-order						
k_1	0.0498	0.0361	0.0374	0.0495	0.0324	0.0211
q_e	3.2572	7.5710	58.981	0.0985	6.8584	4.3636
R^2	0.8863	0.9243	0.8400	0.0714	0.9869	0.9634
Pseudo-second-order						
k_2	0.0339	0.0114	0.00103	0.5768	0.0115	0.01468
q_e	49.875	98.814	152.439	49.925	100	143.47
R^2	1	0.99998	0.99704	1	0.99994	0.99995
Intraparticle diffusion						
k_{id}	0.36838	0.91616	6.73952	0.03392	0.7538	0.54087
C_i	46.4156	89.8709	82.60837	49.7215	92.1957	137.832
R^2	0.67054	0.82085	0.83265	0.24373	0.98736	0.97688
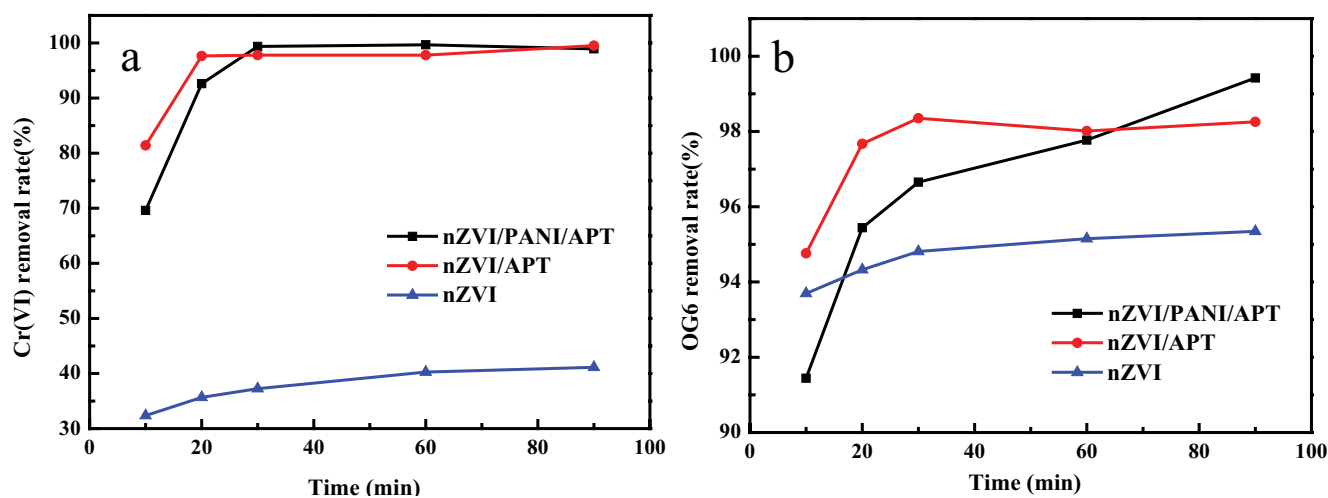
Fig. 4. Effect of different materials on (a) Cr(VI) and (b) OG6 removal performance.
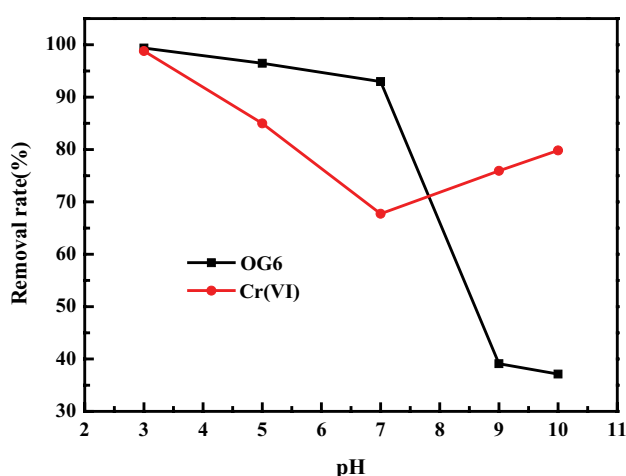

Fig. 5. The effect of solution pH on the Cr(VI) and OG6 removal.

In acidic conditions, the surface of PANI was protonated and Cr(VI) was mainly present in the form of $HCrO_4^-$, $Cr_2O_7^{2-}$ anions [38], which makes electrostatic adsorption between PANI and $HCrO_4^-$, $Cr_2O_7^{2-}$. In addition, the redox reaction of nZVI and Cr(VI) in an acidic solution converts Cr(VI) to Cr(III), increasing the removal efficiency. When the pH > 7, Fe^{2+}, and Fe^{3+} form hydroxide precipitates to lower the amount of Fe^{2+} and Fe^{3+} in the solution, and promotes the redox reaction of nZVI and Cr(VI). So the removal rate of hexavalent chromium is slightly increased. It was observed that OG6 removal slowly decreased at pH = 3–7, followed by a sharp decrease in the pH range of 7–10. The removal of OG6 reached the maximum (99.37%) at pH = 3. This may be attributed to the more dissolved Fe^{2+} and electron production under acidic conditions. Dissolved Fe^{2+} could activate persulfate to generate more sulfate radical anions to oxidize OG6 [39]. In addition, more electrons could reductively cleave the –N=N– of OG6. Nevertheless, under neutral and alkaline conditions,

Fe^{3+} and Fe^{2+} could form iron hydroxide on the surface of nZVI/PANI/APT, hindering the generation and release of Fe^{2+}, while causing the removal efficiency decrease.

3.2.3. Effect of Ps concentration on OG6 and Cr(VI) removal

The differences among nZVI/PANI/APT and nZVI/PANI/APT in the presence of Ps for the simultaneous removal of Cr(VI) and OG6 were investigated. As presented in Fig. 6a, the removal efficiencies of Cr(VI) alone without/with Ps were 97.8%, 70.1% after 90 min, respectively. The lower removal rate of Cr(VI) in the presence of Ps indicated that Ps had a negative effect on the removal of Cr(VI) alone. It was mainly due to the consumption of nZVI by Ps oxidation and suppression of the reduction of Cr(VI). However, the removal efficiency of Cr(VI) alone by nZVI/PANI/APT was nearly equal to that coexistence of Cr(VI) and OG6 by nZVI/PANI/APT with Ps. From Fig. 6b, it is observed that removal efficiencies of OG6 alone without/with Ps were 86.5%, 99.4% after 90 min, respectively, suggesting that added Ps exhibited an important role toward the OG6 removal. Degradation of OG6 only involves the reduction of nZVI due to the absence of Ps, and when Ps are added, both nZVI reduction and free radical oxidation are involved in the OG6 removal resulted in the removal rate increases. It is interesting to note that the presence of Cr(VI) had no negative effect on the removal of OG6 by nZVI/PANI/APT combined Ps system. Furthermore, the removal efficiency of OG6 in coexistence OG6 and Cr(VI) by nZVI/PANI/APT combined Ps system was almost equal to that of OG6 alone. The result confirmed that the simultaneous removal of OG6 and Cr(VI) could be achieved by nZVI/PANI/APT composites in the presence of Ps. It was confirmed that there was a good synergistic effect between nZVI/PANI/APT and persulfate for removal of Cr(VI) and OG6. nZVI not only can be as a reductant for removal Cr(VI) and OG6, but also play as a catalyst to activate Ps and generate sulfate radicals for the removal of OG6.

The effect of Ps on the removal of Cr(VI) and OG6 is presented in Fig. 6c. When the Ps concentrations were
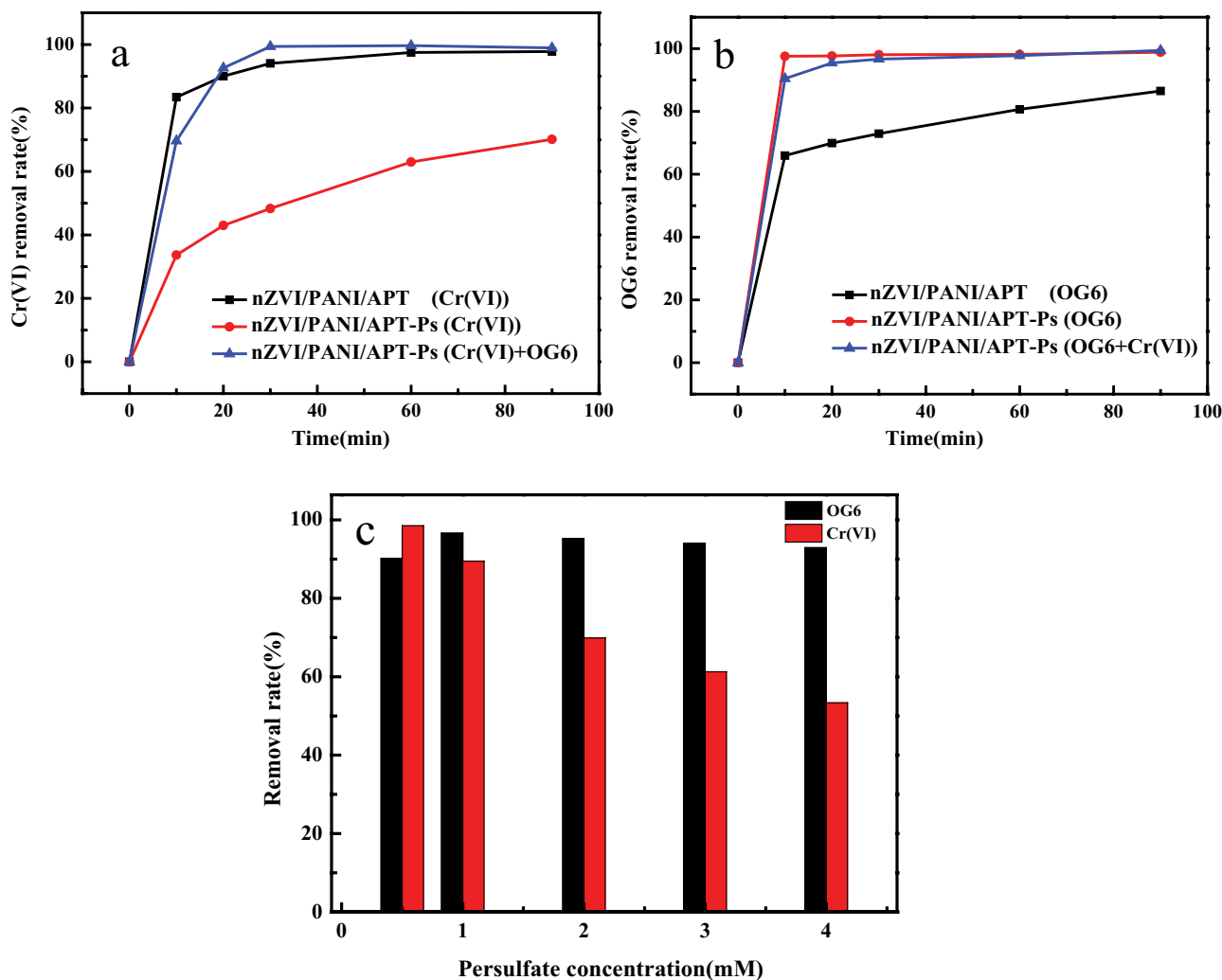
Fig. 6. Removal of (a) Cr(VI) and (b) OG6 by nZVI/PANI/APT and nZVI/PANI/APT-Ps system; Ps concentration on the removal of Cr(VI) and OG6 (c).

1–4 mM, the removal efficiencies of OG6 after 60 min were 90.2%, 96.6%, 95.2%, 94.0%, and 92.9%, respectively. With the increase in the Ps concentration, the removal efficiency of OG6 increased gradually, indicating that the increased amount of Ps could produce sufficient sulfate radicals to degrade OG6 [39]. And when the concentration of Ps exceeded 2 mM, the removal efficiency of OG6 decreased gradually. It declared that the exceeded Ps were detrimental to the degradation of OG6 due to the sulfate radical anions self-scavenging [40]. In addition, the Fe^{2+} can react with sulfate radical anions, which consumes part of the sulfate radical anions lead to the removal rate of OG6 decrease. Moreover, Fig. 6c shows that the removal efficiency of Cr(VI) gradually decreases with the increase of Ps concentration when the reaction time is 60 min, suggested that that the increase of Ps concentration had a negative effect on the Cr(VI) reduction. The increase of Ps concentration results in strengthening the inhibitory effect of persulfate on Cr(VI) removal. It is mainly due to the generated more sulfate radical anions as the increase of Ps concentration. Thus, the formed Cr(III) species would be reconverted into Cr(VI) by sulfate radical anions. In addition, the excess Ps can react with nZVI, which leads to the more consumption nZVI that is insufficient to remove Cr(VI).

3.2.4. Effect of nZVI/PANI/APT dosage and $C_{OG6}/C_{Cr(VI)}$ concentration ratio on the removal of OG6 and Cr(VI)

The effect of dosage on the removal of OG6 and Cr(VI) after a reaction time of 60 min has been researched. The Cr(VI) and OG6 removal increased as the increase of the nZVI/PANI/APT dosage. When the nZVI/PANI/APT dosage exceeded 1.0 g L^{-1}, the Cr(VI) and OG6 removal maintained nearly 97.7% and 98.8%, respectively. The main explanation was that more nZVI/PANI/APT dosage would induce more active sites, and the reaction between nZVI/PANI/APT with Cr(VI) is more likely to occur. At the same time, the increased amount of nZVI/PANI/APT will produce more Fe^{2+} and react with persulfate to produce more sulfate radical oxidative degradation of OG6. Therefore, with the increase of dosage, the removal performance of OG6 also increased.

The results of different concentrations of OG6 on the OG6 and Cr(VI) removal indicated that there were no significant differences were observed in Cr(VI) and OG6 removal within the $C_{OG6}/C_{Cr(VI)}$ concentration ratio range of 1:3–4:3, suggesting that nZVI/PANI/APT had sufficient strong activity for removal Cr(VI) and OG6 completely at 2.00 mM persulfate. It could be interpreted that when the Cr(VI) concentration kept constant, it could lead to the production and consumption of Fe^{2+} remain the same level, and a limited amount of $SO_4^{\cdot-}$ radicals were produced by Fe^{2+} activation of persulfate. Therefore, the OG6 removal performance has no corresponding increased.

3.3. Dynamics study

In order to study the control mechanism of the adsorption process, the different kinetic models were applied such as the pseudo-first-order, the pseudo-second-order, and intraparticle diffusion. The forms of the equations are respectively expressed by using Eqs. (3)–(5), respectively:

$$\ln(q_e - q_t) = \ln q_e - k_1 t \tag{3}$$

$$\frac{t}{q_t} = \frac{1}{k_2 q_e^2} + \frac{t}{q_e} \tag{4}$$

$$q_t = k_{id} t^{1/2} + C_i \tag{5}$$

where k_1 (min^{-1}) is the rate constant of pseudo-first-order model adsorption, k_2 (g (mg min)$^{-1}$) is the rate constant of pseudo-second-order model adsorption, q_e (mg g^{-1}) is the adsorption capacity at equilibrium, q_t (mg g^{-1}) is the adsorption capacity at time t, t (min) is contact time, k_{id} (mg (g min$^{1/2}$)$^{-1}$) is the rate constant of intraparticle diffusion kinetic models and C_i is the boundary layer thickness.

The results of the adsorption kinetics of the composite materials on OG6 and Cr(VI) are shown in Table 3. The results show that the correlation coefficient of the linear fitting of the pseudo-second-order kinetic model is high (R^2 is close to 1), indicating that the pseudo-second-order kinetic model is more suitable for interpreting composite materials than the pseudo-first-order kinetic model and the intraparticle diffusion model. Therefore, it can be concluded that chemisorption is a rate control step in the adsorption process of OG6 and Cr(VI). In addition, the equilibrium adsorption capacity (q_e) calculated by the pseudo-second-order kinetic model is basically consistent with the experimental value.

3.4. Adsorption isotherms study

To understand the adsorption mechanism and interactions between OG6 and Cr(VI) with nZVI/PANI/APT adsorbents, Langmuir, Freundlich and Temkin isotherm models are used to fit the adsorption equilibrium data. Prepare mixed solutions of OG6 and Cr(VI) with different initial concentrations (50–200 mg L^{-1}), add 0.10 g/100 mL adsorbent materials respectively, and oscillate for 2 h at 298, 308, and 318 K, respectively. The equations are as follows:

$$\frac{1}{q_e} = \frac{1}{q_m} + \frac{1}{bq_m C_e} \tag{6}$$

$$\ln q_e = \ln K + \frac{1}{n}\ln C_e \tag{7}$$

$$q_e = B\ln A + B\ln C_e \tag{8}$$

where q_m (mg g^{-1}) is the calculated adsorption capacity at maximum, q_e (mg g^{-1}) is the experimental adsorption capacity at equilibrium, C_e (mg L^{-1}) is the equilibrium concentration of the solution, K (L mg^{-1}) is a Langmuir constant, A (mg L^{-1}) is a Freundlich constant, $B = RT/b$, T is the absolute temperature in Kelvin, R the universal gas constant (8.314 JK^{-1} mol^{-1}), A the equilibrium binding constant, and the constant B is related to the heat of adsorption.

The characteristics of the Langmuir isotherm can be expressed by the Langmuir separation factor (R_L). The R_L reaction is whether the adsorption process is favorable adsorption, and the formula is as follows:

$$R_L = \frac{1}{1 + bC_0} \tag{9}$$

The results of the adsorption isotherm equation of the nZVI/PANI/APT composite on OG6 and Cr(VI) are shown in Table 4. The results show that the Freundlich isotherm equation is more suitable for describing the adsorption process of OG6 and Cr(VI) from the correlation coefficient R^2 (R^2 is close to 1), which means that the adsorption of OG6 and Cr(VI) on the nZVI/PANI/APT surface may be multi-molecular layer adsorption process. The q_m were 75.68 and 90.80 mg g^{-1} for the OG6 and Cr(VI) respectively when the temperature was 318 K.

3.5. Thermodynamic study

In order to better understand the effect of temperature on the adsorption of OG6 and Cr(VI) on composites, adsorption experiments at different temperatures (298, 308 and 318 K, respectively) were carried out to study the change of thermodynamic parameters of OG6 and Cr(VI) adsorption process. The thermodynamic parameters are Gibbs free energy ($\Delta G°$), enthalpy change ($\Delta H°$) and entropy change ($\Delta S°$). The temperatures (298, 308 and 318 K, respectively) were carried out to study the calculation formula is as follows:

$$K_d = \frac{q_e}{C_e} \tag{10}$$

$$\Delta G° = -RTK° \tag{11}$$

$$\ln K° = \frac{\Delta H°}{RT} + \frac{\Delta S°}{R} \tag{12}$$

where q_e is the adsorption capacity (mg g^{-1}) at the equilibrium of adsorption; C_e is the dye concentration (mg L^{-1}) at the equilibrium of adsorption; R is the ideal gas

Table 4
Adsorption isotherm parameters of Cr(VI) and OG6

	Model	Parameters	Temperature (K)		
			298	308	318
OG6	Langmuir	q_{max}	163.7	196.1	202.0
		b	0.2071	0.3597	0.5087
		R_L	0.023	0.013	0.009
		R^2	0.967	0.861	0.935
	Freundlich	K	53.98	63.42	75.68
		n	3.797	2.945	3.073
		R^2	0.987	0.999	0.986
	Temkin	A	1.43×10^{-22}	3.28×10^{-29}	1.77×10^{-36}
		B	0.040	0.029	0.029
		R^2	0.9097	0.9538	0.8810
Cr(VI)	Langmuir	q_{max}	169.8	188.0	193.4
		b	2.1418	0.9981	1.1610
		R_L	0.002	0.005	0.004
		R^2	0.935	0.956	0.944
	Freundlich	K	104.39	94.25	90.80
		n	5.857	4.298	4.136
		R^2	0.948	0.986	0.978
	Temkin	A	3.05×10^{-51}	1.11×10^{-46}	7.29×10^{-45}
		B	0.054	0.040	0.038
		R^2	0.8474	0.8910	0.8765

constant (8.314 J mol^{-1} K^{-1}); K_d is the Langmuir constant (L g^{-1}); T is the temperature (K).

Table 5 shows the calculation results of the thermodynamic parameters of the composite material for the adsorption process of OG6 and Cr(VI). The results show that $\Delta G°$ is negative at different temperatures, indicating that the adsorption process of the complex on OG6 and Cr(VI) is spontaneous. At different temperatures (298, 308, and 318 K), the adsorption process of the composite on OG6 and Cr(VI) is an endothermic reaction, and the elevated temperature is favorable for the reaction.

3.6. Reusability of nZVI/PANI/APT

Regeneration of the nZVI/PANI/APT composite is also an important property for the removal of contaminants from wastewater for the evaluation of its practical usage performance. In this work, regeneration of the composite should be attained by 0.5 mol L^{-1} HCl, water washing and oscillation treatment. The reuse performance of nZVI/PANI/APT on the removal of Cr(VI) and OG6 is shown in Fig. 7. After the nZVI/PANI/APT was reused for five times, the removal efficiency of Cr(VI) from 99.4% dropped to 11.4%. The main reason was that the loss of nZVI increased with the increase of the cycle of reuse and resulted in insufficient reactivity of the composite, therefore the removal rate of Cr(VI) would drop sharply. The removal efficiency of OG6 after regeneration of five times was still up to 73.4%. However, the amount of nZVI decreased, the dissolved Fe^{2+} still activated persulfate to produce sulfate radicals oxidative degradation OG6.

3.7. Discussion of removal mechanism and OG6 degradation pathway

Fig. 8a illustrates the UV-Vis spectra before and after the reaction of OG6 and Cr(VI) with nZVI/PANI/APT in the presence of Ps. 475 nm corresponding to the maximum absorption peak of OG6, 350 nm corresponded to the absorption peak of dichromate ($Cr_2O_7^{2-}$), and 260 nm corresponds to the absorption peak of the $HCrO_4^-$ [5]. It can be seen from the figure that the characteristic peak of OG6 at 475 nm disappeared rapidly with the progress of the reaction, indicating that the chromophore group –N=N– in OG6 was broken, and small molecule compound was formed, which can be degraded by nZVI reduction or Fenton oxidation. The removal of Cr(VI) at 350 nm corresponded to the characteristic peak of $Cr_2O_7^{2-}$ that had substantially disappeared after the reaction. It was mainly due to the redox reaction of Cr(VI) with nZVI under acidic conditions, in which Cr(VI) was the main electron acceptor. The characteristic peak of $HCrO_4^-$ at 260 nm quickly diminished with the reaction, indicating that the hexavalent chromium ion present in the aqueous solution in the form of chromate was degraded.

In the study, besides nZVI reduction, the removal of OG6 was also caused by the oxidation of producing sulfate and hydroxyl radicals with activated Ps. In order to research the effect of sulfate radicals and hydroxyl radicals on the oxidative degradation of OG6, tert-butanol was used as a scavenger for sulfate radicals and hydroxyl radicals, respectively, and ethanol was used as a hydroxyl radical scavenger [41,42]. Preparing the molar ratio of OG6 to ethanol (or tert-butanol) was 1:50 to study the effect of scavenging

Table 5
Adsorption thermodynamic parameters of Cr(VI) and OG6

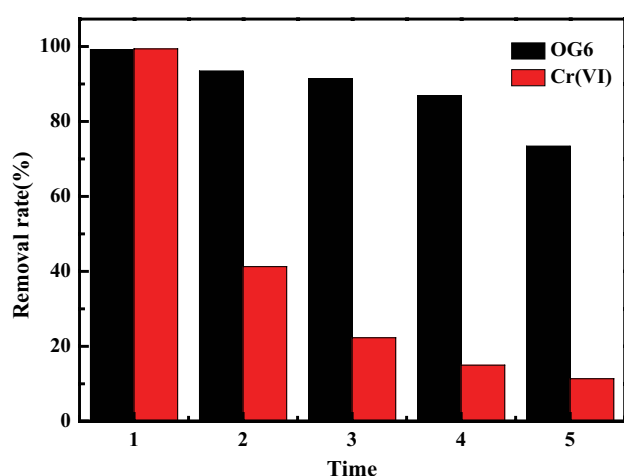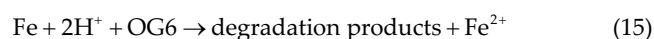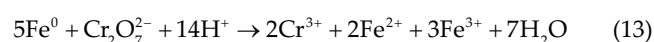|	C_0 (mg L^{-1})	T (K)	K_d (L mg^{-1})	$\Delta G°$ (kJ mol^{-1})	$\Delta H°$ (kJ mol^{-1})	$\Delta S°$ (J mol K^{-1})
OG6	200	298	3.3125	−2.9674	39.9244	145.6177
		308	8.31641	−5.4242		
		318	14.1293	−7.0016		
Cr(VI)	200	298	12.4147	−6.2407	2.3190	28.8623
		308	13.3532	−6.6367		
		318	13.4407	−6.8695		

Fig. 7. Reuse performance of nZVI/PANI/APT on the removal of Cr(VI) and OG6.

on the removal of OG6 and Cr(VI). As shown in Fig. 8b, it can be seen that the removal efficiency of OG6 was 95.4% at 20 min without the addition of scavengers and almost has reached equilibrium, while the removal efficiencies were 84.9% and 77.3% when ethanol and *t*-butanol were added. The equilibrium time for OG6 removal was significantly longer, and the removal efficiency of OG6 was also obviously decreased. The results showed that the sulfate radicals played a role in the removal of OG6, and the hydroxyl radical was also produced. It further confirmed that nZVI reduction and free radical oxidation were involved in the OG6 removal. The scavenger agent had no effect on the removal of Cr(VI), and it indicated that the removal of Cr(VI) was mainly the reduction of nZVI.

In order to analyze and identify the intermediates of degradation of OG6 in the nZVI/PANI/APT-Ps heterogeneous system, the intermediate products after OG6 degradation was determined by high-performance LC-MS. Many different m/z fragments appear in the mass spectrum was helpful to identify the degradation intermediate formation of OG6 and confirmed the oxidative degradation properties of the nZVI surface. The degradation pathway of OG6 was further analyzed as shown in Fig. S2. Since OG6 was oxidized degraded to produce more intermediate products, the main intermediates analyzed by LC-MS were m/z = 194.08 ($C_{10}H_{10}O_4$), m/z = 160.18 ($C_{10}H_8O_2$), m/z = 118.09 ($C_4H_6O_4$), m/z = 96 (SO_4^{2-}), m/z = 90 ($C_2H_2O_4$),

m/z = 62 (NO_3^-) and m/z = 60 ($C_2H_4O_2$). The relative intensity of m/z = 96 (SO_4^{2-}) was the highest, mainly due to the reaction of persulfate with nZVI and Fe^{2+} to produce SO_4^{2-}. According to the test results and related literature reports [5,43,44], a possible pathway for OG6 degradation was proposed. In the first step, OG6 cleaved the azo bond under nZVI and free radicals to form aniline (2) and 7-hydroxy-8-amino-1,3-naphthalene disulfonate (3). In the second step, the aniline was oxidized to a phenol derivative and further oxidized to benzoquinone (6). Further, the 7-hydroxy-8-amino-1,3-naphthalene disulfonate was subjected to desulfonation and oxidation to form 1,2-dihydroxynaphthalene (7). In the third step, benzoquinone was oxidized and ring-opened to form succinic acid (8) and maleic acid (9), and 1,2-dihydroxynaphthalene could be further oxidized to form 1,2-naphthoquinone (10). In the fourth step, succinic acid and maleic acid were oxidized to acetic acid (11) and oxalic acid (12), respectively. In addition, 1,2-naphthoquinone was oxidative cleaved to form 2,2′-(1,2-phenylene)-diacetylacetic acid (13). Finally, the above organic compound can be mineralized into an inorganic compound (H_2O, CO_2, SO_4^{2-} and NO_3^-) by a complicated degradation reaction.

On the basis of the results we analyzed above, the probable mechanism of the simultaneous removal of OG6 and Cr(VI) by nZVI/APT/PANI combined with persulfate system was proposed as follows (1–6): At first, OG6 and Cr(VI) were adsorbed onto PANI/APT surface and the oxide layer of nZVI, while Cr(VI) was reduced into Cr(III) and –N=N– bond of OG6 was breakage by nZVI reduction. In addition, the aqueous Fe^{2+} was more easily released into solution from the nZVI/PANI/APT at acidic conditions. Then generated Fe^{2+} in the reaction process can react with persulfate to produce sulfate and hydroxyl radicals, at the same time, $SO_4^{•-}$ can react with H_2O to produce $HO^•$. Finally, OG6 or the degradation intermediates of OG6 are decomposed into smaller molecules by the strong oxidizing of sulfate and hydroxyl radicals.
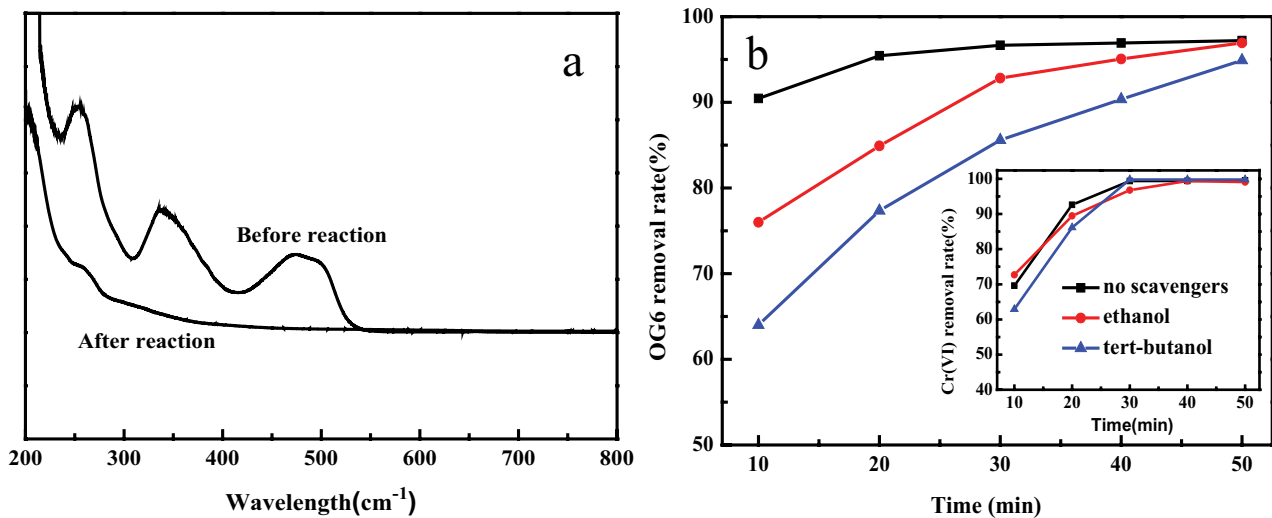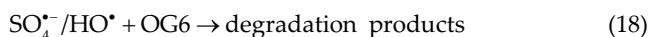
$$5Fe^0 + Cr_2O_7^{2-} + 14H^+ \rightarrow 2Cr^{3+} + 2Fe^{2+} + 3Fe^{3+} + 7H_2O \quad (13)$$

$$2Fe^0 + O_2 + 4H^+ \rightarrow 2Fe^{2+} + 2H_2O \quad (14)$$

$$Fe + 2H^+ + OG6 \rightarrow \text{degradation products} + Fe^{2+} \quad (15)$$

$$Fe^{2+} + S_2O_8^{2-} \rightarrow Fe^{3+} + SO_4^{•-} + SO_4^{2-} \quad (16)$$

Fig. 8. (a) UV-Vis spectra of Cr(VI) and OG6 at degradation before and after and (b) effect of radical scavengers on Cr(VI) and OG6 removal.

$$SO_4^{\bullet -} + H_2O \rightarrow HO^{\bullet} + HSO_4^{-} \qquad (17)$$

$$SO_4^{\bullet -}/HO^{\bullet} + OG6 \rightarrow degradation\ products \qquad (18)$$

4. Conclusions

In this study, the nZVI/PANI/APT composite was prepared by one-step oxidation of aniline with Fe^{3+} as an oxidant and an iron source. The nZVI nanoparticles were loaded on the PANI/APT rod structure, which could effectively disperse the nZVI particles and prevent them from agglomerating, thereby enhancing the reactivity of nZVI. Under pH = 3 acidic conditions, the amount of composite was 1 g/L, and the concentration of Ps = 2 mM, the removal rates of Cr(VI) and OG6 after 60 min were about 99.7% and 99.4%, respectively. The result indicated that the heterogeneous Fenton system had a good catalytic degradation effect on the mixed aqueous solution of heavy metal ions and organic dyes. The removal of Cr(VI) was mainly due to the reduction of nZVI, while the degradation of OG6 was mainly caused by the reduction of nZVI and oxidization of the free radical anions. The adsorption process of OG6 and Cr(VI) were fit well to the Langmuir model and the pseudo-second-order kinetic model, suggesting that adsorption was mainly a single-layer chemisorption process, and thermodynamic parameters estimated that the removal process was an endothermic and spontaneous process. The study showed that nZVI/PANI/APT combined persulfate system has great potential as an efficient adsorbent for water pollution containing heavy metals and organic compounds.

Acknowledgment

References

[1] F.L. Fu, Q. Wang, Removal of heavy metal ions from wastewaters: a review, J. Environ. Manage., 92 (2011) 407–418.
[2] S. Hussain, L. Quinn, J.J. Li, E. Casey, C.D. Murphy, Simultaneous removal of malachite green and hexavalent chromium by *Cunninghamella elegans* biofilm in a semi-continuous system, Int. Biodegrad. Biodeterior., 125 (2017) 142–149.
[3] R. Djellabi, M.F. Ghorab, T. Sehili, Simultaneous removal of Methylene blue and hexavalent chromium from water using $TiO_2/Fe(III)/H_2O_2$/sunlight, CLEAN–Soil Air Water, 45 (2017) 1500379, https://doi.org/10.1002/clen.201500379.
[4] Z.P. Wen, Y.L. Zhang, G. Cheng, Y.R. Wang, R. Chen, Simultaneous removal of As(V)/Cr(VI) and acid orange 7 (AO7) by nanosized ordered magnetic mesoporous Fe-Ce bimetal oxides: behavior and mechanism, Chemosphere, 218 (2019) 1002–1013.
[5] B.-T. Zhang, Y. Zhang, Y.G. Teng, Electrospun magnetic cobalt–carbon nanofiber composites with axis-sheath structure for efficient peroxymonosulfate activation, Sci. Appl. Surf., 452 (2018) 443–450.
[6] Z.A. Alothman, M.M. Alam, Mu. Naushad, Heavy toxic metal ion exchange kinetics: validation of ion exchange process on composite cation exchanger nylon 6,6 Zr(IV) phosphate, J. Ind. Eng. Chem., 19 (2013) 956–960.
[7] L. Xu, L. Yang, X. Bai, X.Y. Du, Y. Wang, P.K. Jin, Persulfate activation towards organic decomposition and Cr(VI) reduction achieved by a novel CQDs-TiO$_2$–*x*/rGO nanocomposite, Chem. Eng. J., 373 (2019) 238–250.
[8] Y. Yang, C. Zhang, D.L. Huang, G.M. Zeng, J.H. Huan, C. Lai, C.Y. Zhou, W.Y. Wang, H. Guo, W.J. Xue, R. Deng, M. Cheng, W.P. Xiong, Boron nitride quantum dots decorated ultrathin porous g-C$_3$N$_4$: intensified exciton dissociation and charge transfer for promoting visible-light-driven molecular oxygen activation, Appl. Catal., B, 245 (2019) 87–99.
[9] X.L. Zou, T. Zhou, J. Mao, X.H. Wu, Synergistic degradation of antibiotic sulfadiazine in a heterogeneous ultrasound-enhanced Fe^0/persulfate Fenton-like system, Chem. Eng. J., 257 (2014) 36–44.
[10] C.J. Liang, C.J. Bruell, M.C. Marley, K.L. Sperry, Persulfate oxidation for in situ remediation of TCE. I. Activated by ferrous

ion with and without a persulfate-thiosulfate redox couple, Chemosphere, 55 (2004) 1213–1223.

[11] S. Rodriguez, A. Santos, A. Romero, F. Vicente, Kinetic of oxidation and mineralization of priority and emerging pollutants by activated persulfate, Chem. Eng. J., 213 (2012) 225–234.

[12] A. Berlin, Kinetics of radical-chain decomposition of persulfate in aqueous solutions of organic compounds, Kinet. Catal., 27 (1986) 34–39.

[13] H. Kusic, I. Peternel, N. Koprivanac, A. Loncaric Bozic, Iron-activated persulfate oxidation of an azo dye in model wastewater: influence of iron activator type on process optimization, J. Environ. Eng., 137 (2011) 454–463.

[14] B.T. Zhang, Y. Zhang, W.X. Xiang, Y.-G. Teng, Y. Wang, Comparison of the catalytic performances of different commercial cobalt oxides for peroxymonosulfate activation during dye degradation, Chem. Res. Chin. Univ., 33 (2017) 822–827.

[15] E. Saputra, S. Muhammad, H.Q. Sun, H.M. Ang, M.O. Tadé, S.B. Wang, Different crystallographic one-dimensional MnO_2 nanomaterials and their superior performance in catalytic phenol degradation, Environ. Sci. Technol., 47 (2013) 5882–5887.

[16] S. Rodriguez, L. Vasquez, D. Costa, Oxidation of orange G by persulfate activated by Fe(II), Fe(III) and zero valent iron (ZVI), Chemosphere, 101 (2014) 86–92.

[17] Z.-H. Diao, X.-R. Xu, H. Chen, D. Jiang, Y.-X. Yang, L.-J. Kong, Y.-X. Sun, Y.-X. Hu, Q.-W. Hao, L. Liu, Simultaneous removal of Cr(VI) and phenol by persulfate activated with bentonite-supported nanoscale zero-valent iron: reactivity and mechanism, J. Hazard. Mater., 316 (2016) 186–193.

[18] F.L. Fu, D.D. Dionysiou, H. Liu, The use of zero-valent iron for groundwater remediation and wastewater treatment: a review, J. Hazard. Mater., 267 (2014) 194–205.

[19] Z.M. Sun, S.L. Zheng, G.A. Ayoko, R.L. Frost, Y.F. Xi, Degradation of simazine from aqueous solutions by diatomite-supported nanosized zero-valent iron composite materials, J. Hazard. Mater., 263 (2013) 768–777.

[20] L.-N. Shi, X. Zhang, Z.-L. Chen, Removal of chromium(VI) from wastewater using bentonite-supported nanoscale zero-valent iron, Water Res., 45 (2011) 886–892.

[21] Z.X. Chen, T. Wang, X.Y. Jin, Z.L. Chen, M. Megharaj, R. Naidu, Multifunctional kaolinite-supported nanoscale zero-valent iron used for the adsorption and degradation of crystal violet in aqueous solution, J. Colloid Interface Sci., 398 (2013) 59–66.

[22] B. Mu, A.Q. Wang, Adsorption of dyes onto palygorskite and its composites: a review, J. Environ. Chem. Eng., 4 (2016) 1274–1294.

[23] R.L. Frost, Y.F. Xi, H.P. He, Synthesis, characterization of palygorskite supported zero-valent iron and its application for methylene blue adsorption, J. Colloid Interface Sci., 341 (2010) 153–161.

[24] S. Giri, M. Bhaumik, R. Das, V.K. Gupta, A. Maity, Dehalogenation of aromatic halides by polyaniline/zero-valent iron composite nanofiber: kinetics and mechanisms, Appl. Catal., B, 202 (2017) 207–216.

[25] H. Xu, W.G. Tian, Y.J. Zhang, J. Tang, Z.T. Zhao, Y. Chen, Reduced graphene oxide/attapulgite-supported nanoscale zero-valent iron removal of acid red 18 from aqueous solution, Water Air Soil Pollut., 12 (2018) 229.

[26] H.L. Lu, H. Xu, Y. Chen, J.L. Zhang, J.X. Zhuang, ZVI/PANI/ATP composite by static polymerization as adsorbent for removal of Cr(VI), RSC Adv., 4 (2014) 5873–5879.

[27] Y.C. Yin, M. Zeng, J. Liu, W.K. Tang, H.R. Dong, R.Z. Xia, R.H. Yu, Enhanced high-frequency absorption of anisotropic Fe_3O_4/graphene nanocomposites, Sci. Rep., 6 (2016) 25075.

[28] J.X. Xu, W.B. Wang, A.Q. Wang, Effects of solvent treatment and high-pressure homogenization process on dispersion properties of palygorskite, Powder Technol., 235 (2013) 652–660.

[29] R. El-Tawil, S. El-Wakeel, A. Abdel-Ghany, H.A.M. Abuzeid, K.A. Selim, A.M.A. Hashem, Silver/quartz nanocomposite as an adsorbent for removal of mercury(II) ions from aqueous solutions, Heliyon, 5 (2019) e02415.

[30] F. Akti, M. Okur, The removal of acid violet 90 from aqueous solutions using PANI and PANI/clinoptilolite composites: isotherm and kinetics, J. Polym. Environ., 26 (2018) 4233–4242.

[31] C.J. Jin, J. Han, F.Y. Chu, X.X. Wang, R. Guo, Fe_3O_4@PANI hybrid shell as a multifunctional support for Au nanocatalysts with a remarkably improved catalytic performance, Langmuir, 33 (2017) 4520–4527.

[32] X. Liu, X.T. Xu, J. Sun, A. Alsaedi, T. Hayat, J.X. Li, X.K. Wang, Insight into the impact of interaction between attapulgite and graphene oxide on the adsorption of U(VI), Chem. Eng. J., 343 (2018) 217–224.

[33] B. Mu, A.Q. Wang, One-pot fabrication of multifunctional superparamagnetic attapulgite/Fe_3O_4/polyaniline nanocomposites served as an adsorbent and catalyst support, J. Mater. Chem. A, 3 (2015) 281–289.

[34] B. Rhouta, E. Zatile, L. Bouna, O. Lakbita, F. Maury, M.C. Lafont, M.B. Amjoud, F. Senocq, A. Jada, A.A. Aghzzaf, Comprehensive physicochemical study of dioctahedral palygorskite-rich clay from Marrakech High Atlas (Morocco), Phys. Chem. Miner., 40 (2013) 411–424.

[35] H. Xu, J.X. Wu, C.L. Li, J.L. Zhang, J.Y. Liu, Investigation of polyaniline films doped with Fe^{3+} as the electrode material for electrochemical supercapacitors, Electrochim. Acta, 165 (2015) 14–21.

[36] R. Das, M. Bhaumik, S. Giri, A. Maity, Sonocatalytic rapid degradation of Congo red dye from aqueous solution using magnetic Fe(0)/polyaniline nanofibers, Ultrason. Sonochem., 37 (2017) 600–613.

[37] W.C. Cheng, C.C. Ding, X.X. Wang, Z.Y. Wu, Y.B. Sun, S.H. Yu, T. Hayat, X.K. Wang, Competitive sorption of As(V) and Cr(VI) on carbonaceous nanofibers, Chem. Eng. J., 293 (2016) 311–318.

[38] C.X. Zhang, Y.B. Sun, Z.Q. Yu, G. Zhang, J.W. Feng, Simultaneous removal of Cr(VI) and acid orange 7 from water solution by dielectric barrier discharge plasma, Chemosphere, 191 (2018) 527–536.

[39] X.Y. Wei, N.Y. Gao, C.J. Li, Y. Deng, S.Q. Zhou, L. Li, Zero-valent iron (ZVI) activation of persulfate (Ps) for oxidation of bentazon in water, Chem. Eng. J., 285 (2016) 660–670.

[40] K.F. Shang, X.J. Wang, J. Li, H. Wang, N. Lu, N. Jiang, Y. Wu, Synergetic degradation of Acid orange 7 (AO7) dye by DBD plasma and persulfate, Chem. Eng. J., 311 (2017) 378–384.

[41] Y.F. Ji, C. Ferronato, A. Salvador, X. Yang, J.-M. Chovelon, Degradation of ciprofloxacin and sulfamethoxazole by ferrous-activated persulfate: implications for remediation of groundwater contaminated by antibiotics, Sci. Total Environ., 472 (2014) 800–808.

[42] G.P. Anipsitakis, D.D. Dionysiou, Radical generation by the interaction of transition metals with common oxidants, Environ. Sci. Technol., 38 (2004) 3705.

[43] C.-F. Liu, C.P. Huang, C.-C. Hu, C.P. Huang, A dual TiO_2/Ti-stainless steel anode for the degradation of orange G in a coupling photoelectrochemical and photo-electro-Fenton system, Sci. Total Environ., 659 (2019) 221–229.

[44] L.C. Almeida, B.F.-Silva, M.V.B. Zanoni, Photoelectrocatalytic/photoelectro-Fenton coupling system using a nanostructured photoanode for the oxidation of a textile dye: kinetics study and oxidation pathway, Chemosphere, 136 (2015) 63–71.
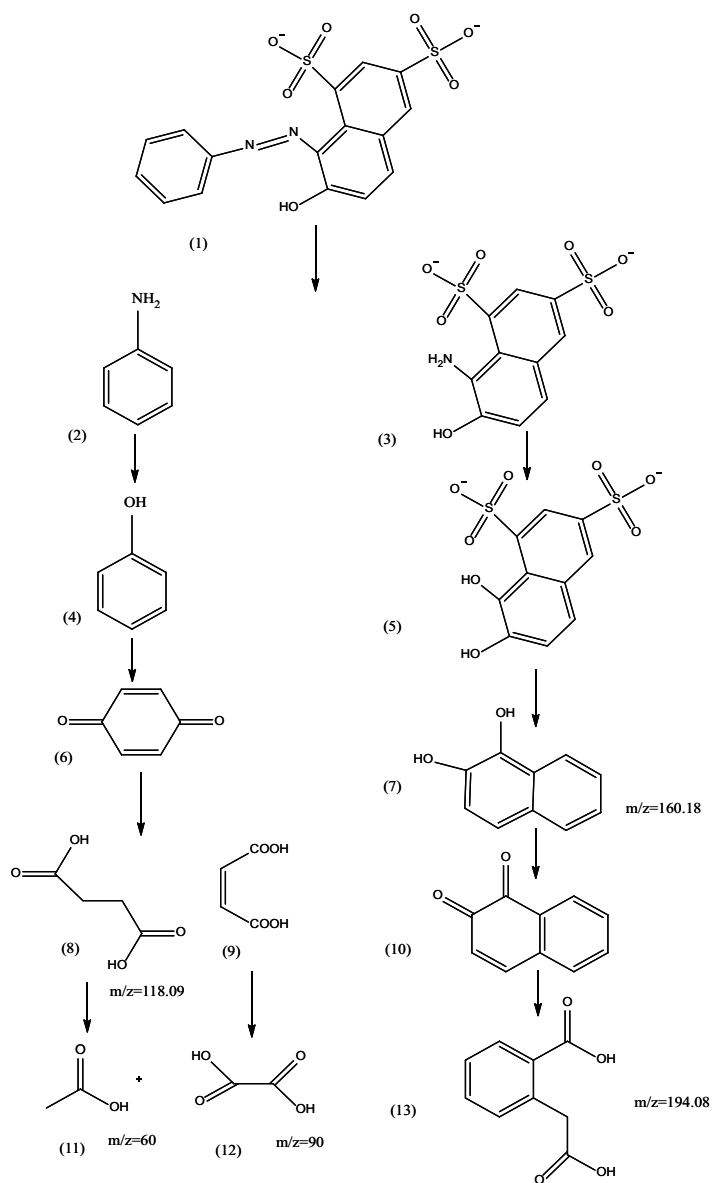
Supplementary information

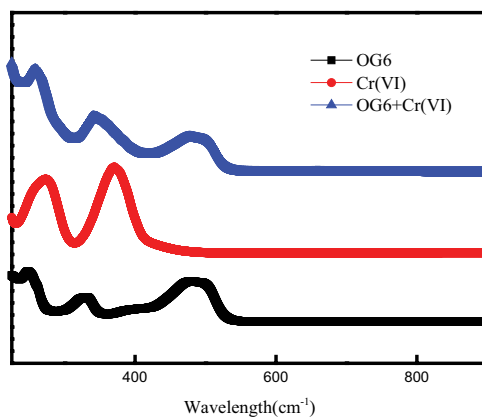Fig. S1. The proposed degradation pathway of OG6.

Fig. S2. UV-Vis spectrum of OG6 and Cr(VI) alone and before the reaction of the mixture.